Article:
Beicker, CLL, Amjad, M, Bandarra Filho, EP et al. (1 more author) (2018) Experimental study of photothermal conversion using gold/water and MWCNT/water nanofluids. Solar Energy Materials and Solar Cells, 188. pp. 51-65. ISSN 0927-0248

https://doi.org/10.1016/j.solmat.2018.08.013

Experimental Study of Photothermal Conversion using Gold/water and MWCNT/water nanofluids

Carolina L. L. Beicker[1], Muhammad Amjad[2,3], Enio P. Bandarra Filho[1*], Dongsheng Wen[4.3]

[1]Energy and Thermal Systems Laboratory, Faculty of Mechanical Engineering, Federal University of Uberlandia, Brazil

[2]Department of Mechanical, Mechatronics and Manufacturing Engineering (KSK Campus), University of Engineering and Technology Lahore, Pakistan

[3]School of Chemical and Process Engineering, University of Leeds, Leeds, U.K

[4]School of Aeronautic Science and Engineering, Beihang University, Beijing, P.R.China

Emails: carolina.beicker@ufu.br, bandarra@ufu.br;

Address: Federal University of Uberlandia, School of Mechanical Engineering, Av. Joao Naves de Avila, 2121 – Santa Monica, Uberlandia, MG 38400-902, Brazil

Abstract

This work experimentally investigated photothermal conversion behavior of Gold/water and MWCNT/water nanofluids at different volumetric concentrations (0.0001%-0.004% and 0.0001%-0.03%, respectively). The experiments were conducted for ~10 hours outdoor on each test day, without interruptions. The results show that the tested nanofluids have excellent photothermal conversion capability even under very low concentrations. Specific absorption rate (SAR) presented an exponential decay with increasing volumetric concentration of nanoparticles in the sample while both the total

energy stored by the fluid sample during the heating period and the stored energy ratio (SER) increased with the increase in nanoparticles concentration. The results indicates the existence of an “optimal” volumetric concentration, above which further nanoparticle addition becomes indifferent or infeasible. This optimal nanoparticle volumetric concentration was found to be 0.002% for the gold nanofluid and 0.001% for the MWCNT samples.

Keywords:

Photothermal conversion, nanofluid, SAR, stored energy, direct absorption

Abbreviations

bf: base fluid
CNT: Carbon Nanotubes
CPC: Compound Parabolic Concentrator
Dir: Direction
ETSC: Evacuated Tube Solar Collector
f: fluid
FPSC: Flat Plate Solar Collector
Inst: Instantaneous
LSPR: Localized Surface Plasmon Resonance
MWCNT: Multi-Walled Carbon Nanotubes
nf: nanofluid
np: nanoparticle
PSC: Parabolic Solar Collector
SAR: Specific Absorption Rate
SER: Stored Energy Ratio
SWCNT: Single-Walled Carbon Nanotubes
Vel: Velocity
VSAR: Volumetric Specific Absorption Rate

1 Introduction

Solar energy is a renewable source widely used for heating purposes and becomes more and more important for our future energy supply. For solar heating applications, collectors rely on black or selective surfaces for the absorption of incident radiation, and transfer of the absorbed heat to a working fluid flows inside tubes. The solar heating process that occurs on these traditional systems are not as efficient as it should be, since there are at least three different thermal resistances between the solar radiation incidence and the working fluid heating: radiation absorption by the solar absorber, conduction heat transfer from the absorber to the tubes, and convection from the tubes to the working fluid.

The first practical idea of a system projected to overcome the limitations of the traditional collectors was originated in the 1970's. It was based on the concept of direct absorption of solar radiation by a fluid, promising to increase the absorbed energy and reduce heat losses to the ambient. The propose was to reply the absorber surface and metal pipes by a transparent cover or pipes with running fluids inside, which absorbs solar energy directly in the liquid phase, transforming the heat transfer process into a volumetric phenomenon. One of the pioneer reports of such work is from Minardi and Chuang (1974), who used a so-called "highly absorbent black liquid" to capture solar energy in transparent channels. Years later, with the advances in measurements technology, it was possible to discover that the type of fluid used by Minardi and Chuang (1974), an India Ink, very like China Ink properties, was a type of nanoscale particle dispersion (Swider et al., 2003). Later, Arai et al. (1984) experimentally tested a "volume heat-trap type solar collector" using a fine-particle semitransparent liquid

suspension to enhance the efficiency. These prior works using very small particles (nanometer scale) dispersed on different liquids opened many possibilities, which has challenged researchers on obtaining stable "nanofluids", a term first used by Choi and Eastman (1995). Intensive interest in nanofluids has been received in past years and many progresses have been made. The advances in production techniques make it easier to produce a wide variety of nanofluids, especially for the two-step production method, in which nanoparticles can be obtained from a wide range of materials at higher quantities and lower cost (step one) and then dispersed in selected liquids (step two), Wen et al. (2009).

Among the recent experimental studies in photothermal conversion using nanofluids, a wide range of nanofluids were produced from metal, oxides and carbon-based nanoparticles and dispersed in water, ethylene glycol, propylene glycol and Therminol VP1, as shown in Table 1.

Table 1 – Nanoparticles and base fluids used in recent experimental studies

Authors	**Nanoparticle**	**Base Fluid**	**Subject**	**Type of study**
Otanicar et al. (2010)	Graphite, CNT, Ag	Water	Application: micro-solar-thermal-collector	Experimental
Taylor et al. (2011a)	Al, Ag, Cu, Graphite	Therminol VP1	Optical properties/ Application: PSC	Theoretical - Experimental
Taylor et al. (2011b)	Al, Au, Ag, Graphite, Cu, TiO_2	Water, Therminol VP1	Optical properties	Theoretical - Experimental
He et al. (2011)	TiO_2, MWCNT	Water	Application: ETSC	Experimental
Lenert and Wang (2012)	Co-Carbon	Therminol VP1	Optimization: volumetric receiver using	Theoretical - Experimental

			concentrated solar radiation	
Yousefi et al. (2012a)	Al_2O_3	Water	Application: FPSC	Experimental
Yousefi et al. (2012b)	MWCNT	Water	Application: FPSC	Experimental
Yousefi et al. (2012c)	MWCNT	Water	Application: FPSC	Experimental
Khullar et al. (2012)	Al	Therminol VP1	Application: PSC	Experimental
He et al. (2013)	Cu	Water	Photothermal properties	Experimental
Jamal-Abad et al. (2013)	Cu	Water	Application: FPSC	Experimental
Liu et al. (2013)	CuO	Water	Application: evacuated tubular solar air collector with CPC	Experimental
He et al (2014)	Cu	Water	Application: FPSC	Experimental
Hordy et al. (2014)	MWCNT	Water, ethylene glycol, Therminol VP1, propylene glycol	Application: solar collector	Experimental
Bandarra Filho et al. (2014)	Ag	Water	Photothermal conversion efficiency	Experimental
Karami et al. (2014)	CNT	Water	Photothermal properties	Experimental
Zhang et al. (2014)	Au	Water	Photothermal conversion efficiency	Experimental
Gupta et al. (2015)	AL_2O_3	Water	Application: DASC	Experimental
Karami et al. (2015)	CuO	Water-ethylene glycol	Application: DASC	Experimental
Sabiha et al. (2015)	SWCNT	Water	Application: ETSC	Experimental
Salavati Meibodi	SiO_2	Water-ethylene	Application:	Experimental

et al. (2015)		glycol	FPSC	
Tong et al. (2015)	MWCNT	Water	Application: U tube solar collector	Experimental
Delfani et al. (2016)	MWCNT	Water-ethylene glycol	Application: DASC	Experimental
Vakili et al. (2016)	Graphene	Water	Application: DASC	Experimental
Verma et al. (2016)	MgO	Water	Application: FPSC	Experimental
Vincely e Natarajan (2016)	Graphene oxide	Water	Application: FPSC	Experimental
Jeon et al. (2016)	Au	Water	Application: FPSC	Theoretical - Experimental
Chen et al. (2016)	Au	Water	Application: DASC	Experimental
Amjad et al. (2017)	Au	Water	Photothermal conversion efficiency	Experimental
Fu et al. (2017)	Graphene oxide-Au	Water	Application: Solar vapor generation	Experimental
Rose et al. (2017)	Graphene oxide	Ethylene Glycol	Optical properties	Theoretical - Experimental
Iranmanesh et al. (2017)	Graphene	Water	Application: ETSC	Experimental
Chen et al. (2017)	Au	Water	Photothermal conversion efficiency	Theoretical - Experimental
Wang et al. (2018)	Chinese ink Cu, CuO, Carbon Black	Water	Photothermal conversion efficiency	Experimental
Mahbudul et al. (2018)	SWCNT	Water	Application: ETSC	Experimental
Duan et al. (2018)	Au, SiO_2 cores coated with Au nanoshell	Water	Photothermal conversion efficiency	Theoretical
Liu et al. (2018)	Reduced Graphene Oxide	Water	Application: Solar vapor generation	Experimental

The use of plasmonic nanoparticles (nanoparticles produced from noble metal) have been highlighted for photothermal conversion applications due to their improved absorptivity, provided by the Localized Surface Plasmon Resonance (LSPR), a phenomenon of resonant energy transfer from incident light photons to the free electrons present in the metal surface. This resonance, for noble metals, occurs in the frequencies of visible light and enhance the photothermal conversion efficiency of plasmonic nanofluids. (Bandarra Filho et al., 2014; Zhang et al, 2014; Chen et al., 2015; Du and Tang, 2016, Jeon et al., 2016; Chen et al., 2016; Amjad et al., 2017; Chen et al., 2017; Duan et al., 2018)

Carbon-based nanoparticles have also been reported by many authors as potential candidates for use in solar collectors, especially for low to medium temperature applications (<400 ºC) due to their high spectral absorptivity over the entire solar range, low cost compared with other nanoparticle's material and good photothermal conversion efficiency even at low concentrations (He et al., 2011; Taylor et al., 2011a; Taylor et al. 2011b; Ladjevardi et al., 2013; Hordy et al., 2014; Sabiha et al., 2015; Delfani et al., 2016; Vakili et al., 2016, Iranmanesh et al., 2017; Wang et al., 2018; Mahbudul et al., 2018).

Recent results show that, despite of great nanoparticle optical characteristics and proven enhancement on photothermal conversion efficiency presented, its appropriate application depends mostly on many factors of the whole system : pH of the sample (Yousefi et al., 2012c), fluid depth (Taylor et al., 2011b; Lenert and Wang, 2012, Liu et al., 2018), nanoparticle size and aspect ratio (Otanicar et al., 2010; He et al, 2014; Du and Tang, 2016) and, mostly reported, nanoparticle concentration (Tyagi et al., 2009; Otanicar et al., 2010; Khullar e Tyagi, 2010; Taylor et al., 2011b; He et al., 2011; Lenert e Wang, 2012; Yousefi et al., 2012a; Ladjevardi et al., 2013; He et al., 2013; Liu et al.,

2013; Gupta et al., 2015; Verma et al., 2016; Du and Tang, 2016; Liu et al., 2018), as well as economy and cost issues. These results show that future applications using nanofluids as solar radiation absorbers will have to overcome the optimization problem since the use of specific nanofluids in a system with, for example, an inappropriate nanoparticle concentration, may not lead to better results.

It shall be noted that most of these studies were based on solar simulators using small sample volumes, which cannot represent real application environment. Various nanoparticles were investigated under different conditions, which made the assessment the performance of different nanoparticles difficult. In order to advance our understanding of the influence of the nanoparticle type and concentration, this work assessed the photothermal performance of MWCNT/water and Gold/water samples at different volume fractions under realistic conditions. To reach a fair comparison, all samples were exposed to outdoor sunlight at the same time for about 10 hours (from sunrise to sunset) under natural solar radiation. The influence of particle type and concentration on the photothermal conversion efficiency, and the samples stability after the experiments were also discussed.

2 Material and Methods

2.1 Nanofluid Preparation

In the present study, several nanofluids samples were produced from two different materials: gold nanoparticles and multi-walled carbon nanotubes (referred here as, MWCNT or, simply, CNT), both dispersed in distillated water. A gold nanofluid sample with high concentration was synthesized by a modified thermal citrate reduction (the details about the synthesis and characterization can be found in Amjad et al.

(2017)) and a high concentrated MWCNT nanofluid was bought from NanoAmor (Nanostructured & Amorphous Materials, Inc.).

Table 2 – Characteristics of the primary nanofluids used in the present work.

Nanoparticle type	Nanoparticle format	ρ_{np} (g/cm³)	Nanoparticle size	Base fluid	Φ_w (%)	ϕ_v (%)
Gold	Spherical	19.3	Diameter 10-30 nm	Distilled water	0.2896	0.015
MWCNT	Tubular, with multiple walled	2.1	Outside Diameter 50-80 nm Inside Diameter 5-15 nm Lenght 10-20 µm	Distilled water	9	4.485

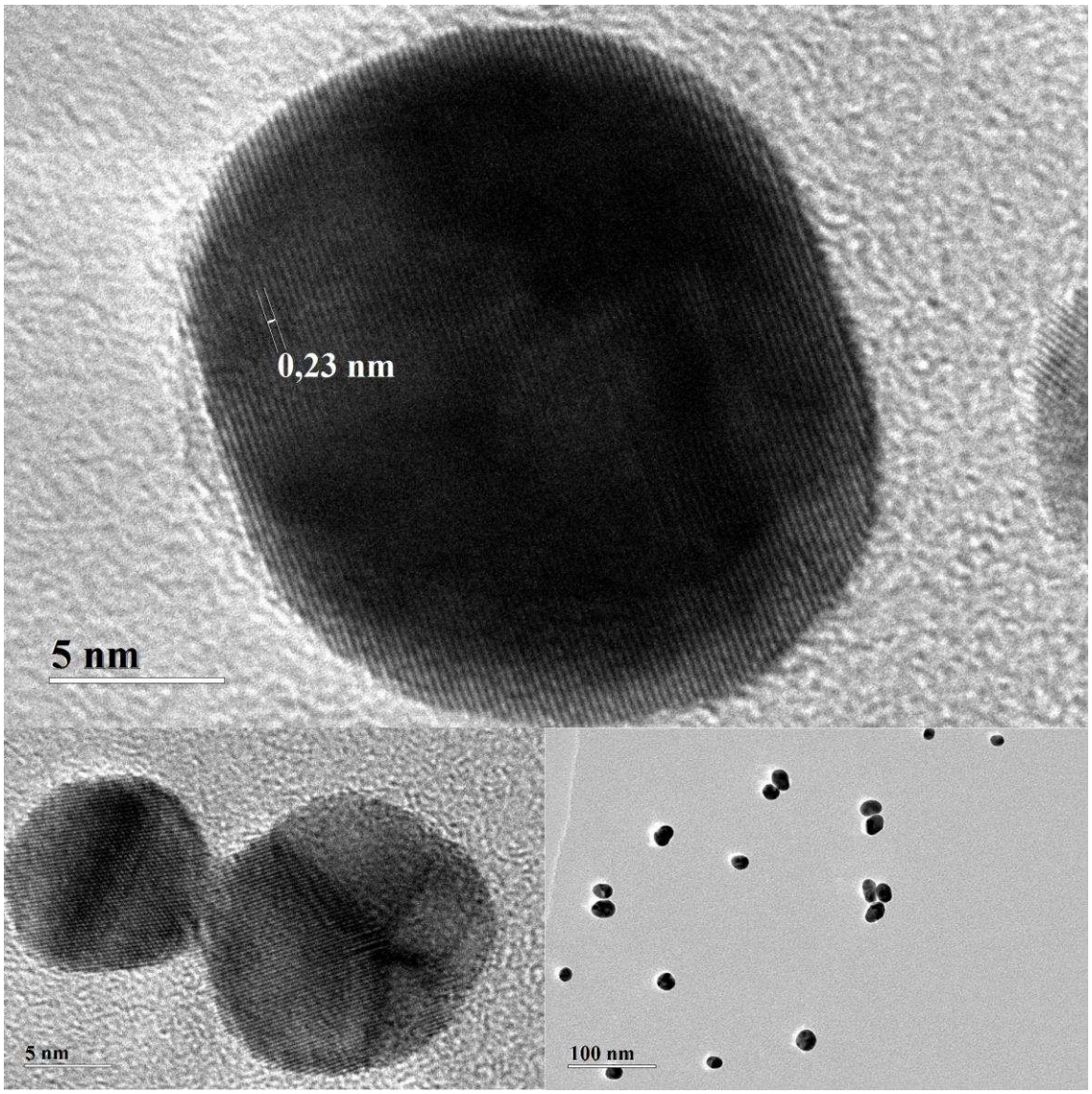

(a)

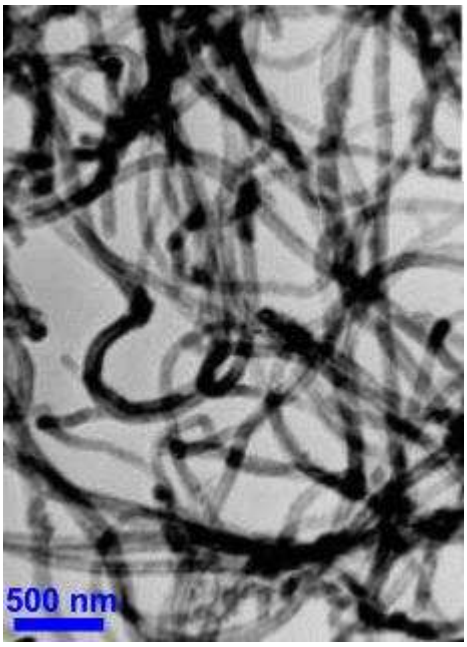

(b)

Fig. 1 TEM images of (a) gold nanofluid sample (b)MWCNT sample.

The two high concentrated nanofluids, described in Table 2 and represented by Fig. 1, were used to obtain volumetric concentrations varying from 0.0001 to 0.0040% for the gold nanofluids samples and from 0.0001 to 0.3% for the MWCNT samples. The final nanofluids were obtained by a process of addition of water to higher concentration samples followed by a 20 minutes sonication process, as shown in Fig. 2.

Fig. 2 Sonication process of a gold nanofluid sample.

2.2 Experimental Setup

A schematic diagram of the experimental system used in the present investigation is shown in Fig. 3. The test system included a support with the capacity of installing twelve test cells. The rectangular-shaped cells were made mainly from two transparent acrylic glasses with dimensions of 120 (L) x 140 (H) x 5 (D) mm, separated by a gap of 10 mm, as shown in Fig. 4. To reduce heat loss, thermal insulation material was used in the opposite face of solar incidence and, for better accuracy in the temperature measurements, thermocouples holders were specially designed to guarantee the position of the sensors at the central position of fluid volume. 30 AWG T type thermocouples were logged into a data acquisition system linked to a PC under a Labview platform.

The thermocouples were calibrated in an ultra cryostatic circulating bath using a NIST traceable precision glass thermometer with a precision of ±0.01 ºC and the uncertainties were determined as 0.1 ºC, according to the procedure suggested by Abernethy and Thompson (1980), with an interval of confidence of 95%.

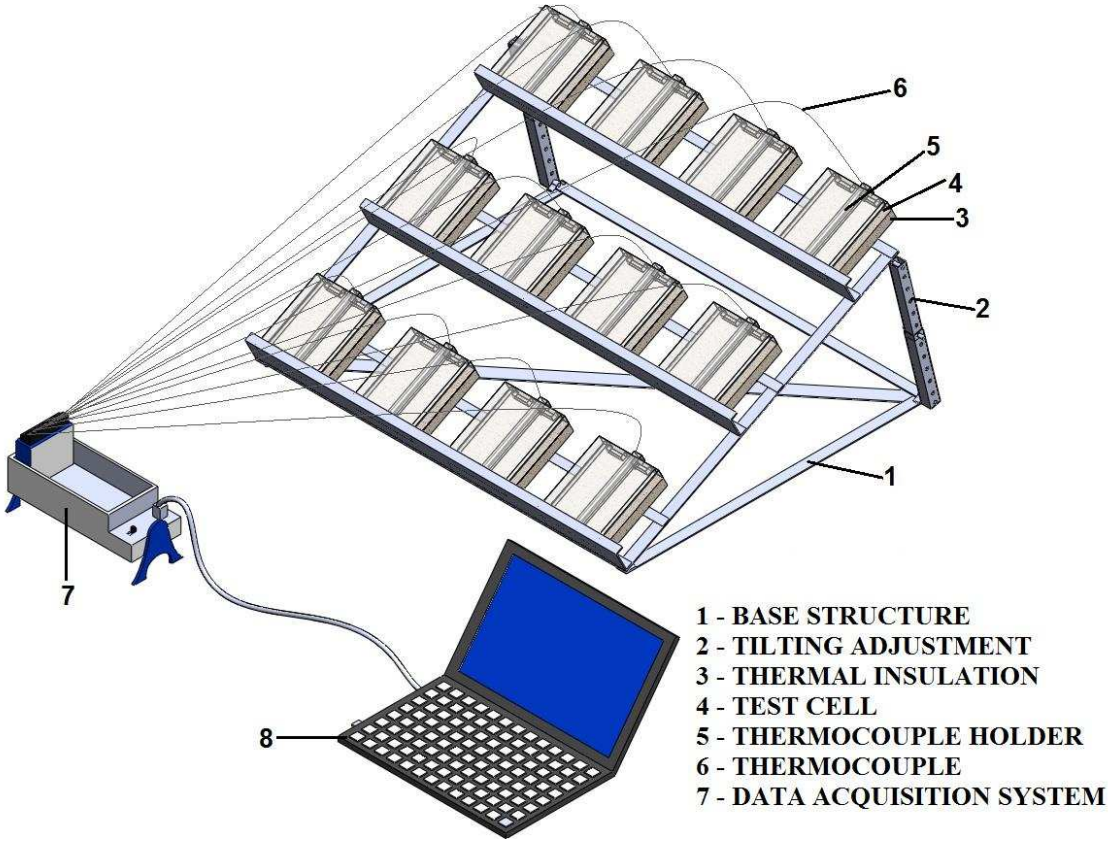

(a)

(b)

Fig. 3 Experimental system: (a) a schematic illustration and (b) a snapshot of the system under direct sunlight on top of a roof.

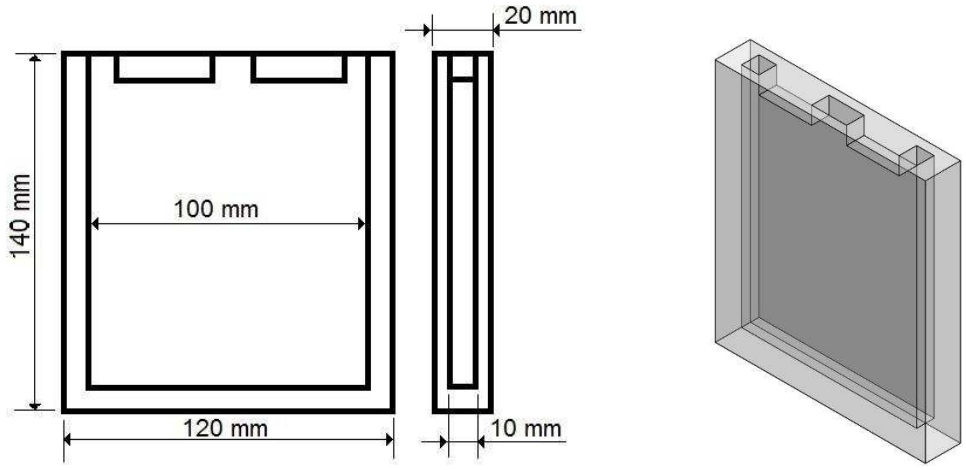

(a) (b)

Fig. 4 Acrylic containers used in the tests. (A) Views and dimensions. (B) Three-dimensional view.

2.3 Experimental Procedure

The experiments were performed with pre-defined conditions: orientation of the base structure, as shown in Fig. 5; sample volume, defined as 100 ml (without refill or replacement between each testing day); and thermocouple position, defined as the central position of the tested fluid. The orientation and tilt angle adjustment of the system was performed according to ABNT NBR 15569:2008 standard for the maximum collector efficiency on a whole year use installation. Extensive tests were carried out for each type of nanofluid with a daily duration of approximately eight hours starting at 7:00 AM. One representative test result will be presented in the following sections for each nanofluid and the weather conditions of these days of test are presented in Tables 3 and 4 and the solar radiation intensity during the representative testing days are presented in figures 6 and 7.

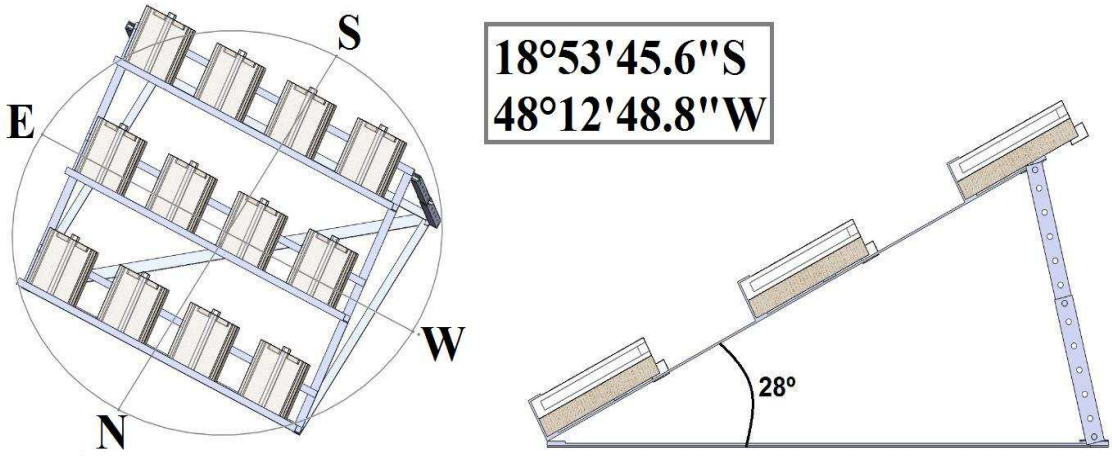

Fig. 5 – Base structure localization, orientation and selected tilt angle.

Table 3 - Local weather condition corresponding to the representative day of test with gold nanofluids

Date	Local	Temperature (°C)	Humidity (%)	Wind (m/s)	Radiation

	Time	Inst.	Max.	Min.	Inst.	Max.	Min.	Vel.	Dir.	(kJ/m²)
06/05	7	18.5	18.6	18.2	61	62	59	1.6	73°	17.78
06/05	8	20.7	20.8	18.5	58	62	57	1.3	48°	458.2
06/05	9	24.3	24.4	20.7	47	58	47	1.7	44°	1245
06/05	10	25.7	25.9	24.3	44	48	43	2.7	21°	1862
06/05	11	26.9	27.7	25.4	42	46	41	3.6	11°	2503
06/05	12	28.7	28.9	26.9	36	42	36	2.8	29°	2899
06/05	13	27.8	28.7	27.1	34	38	32	2.8	27°	2339
06/05	14	28.6	28.7	27.5	32	34	31	2.4	5°	2107
06/05	15	28.2	29.2	28.0	31	32	29	2.1	27°	2038
06/05	16	28.6	28.7	28.0	31	32	31	1.9	13°	1168
06/05	17	27.6	28.9	27.6	33	33	30	2.3	37°	872.3
06/05	18	27.0	28.4	27.0	34	35	32	1.2	28°	308.9

Table 4 - Local weather condition corresponding to the representative day of test with MWCNT nanofluids (partly cloudy weather condition)

Date	Local Time	Temperature (°C)			Humidity (%)			Wind (m/s)		Radiation (kJ/m²)
		Inst.	Max.	Min.	Inst.	Max.	Min.	Vel.	Dir.	
28/05	7	18.3	18.4	18.2	67	68	66	2.7	79°	1.54
28/05	8	19.1	19.1	18	64	69	64	2.7	75°	225.2
28/05	9	21.5	21.5	19.1	52	64	52	3.7	85°	1065
28/05	10	24.0	24.0	21.5	46	53	46	3.9	83°	1932
28/05	11	25.3	25.3	23.7	44	47	44	3.3	71°	2242
28/05	12	25.6	26.5	24.9	41	44	40	3.2	39°	2522
28/05	13	26.3	26.6	25.4	41	43	38	2.8	55°	2435
28/05	14	26.7	26.9	25.6	38	44	37	2.5	64°	2378
28/05	15	26.8	27.1	26.2	36	40	35	2.8	60°	2156
28/05	16	26.6	27.4	26.5	35	37	32	1.9	49°	1601
28/05	17	26.3	27.1	26.0	37	38	33	1.4	66°	724.6
28/05	18	25.0	26.5	25.0	41	41	36	2.1	84°	203.4

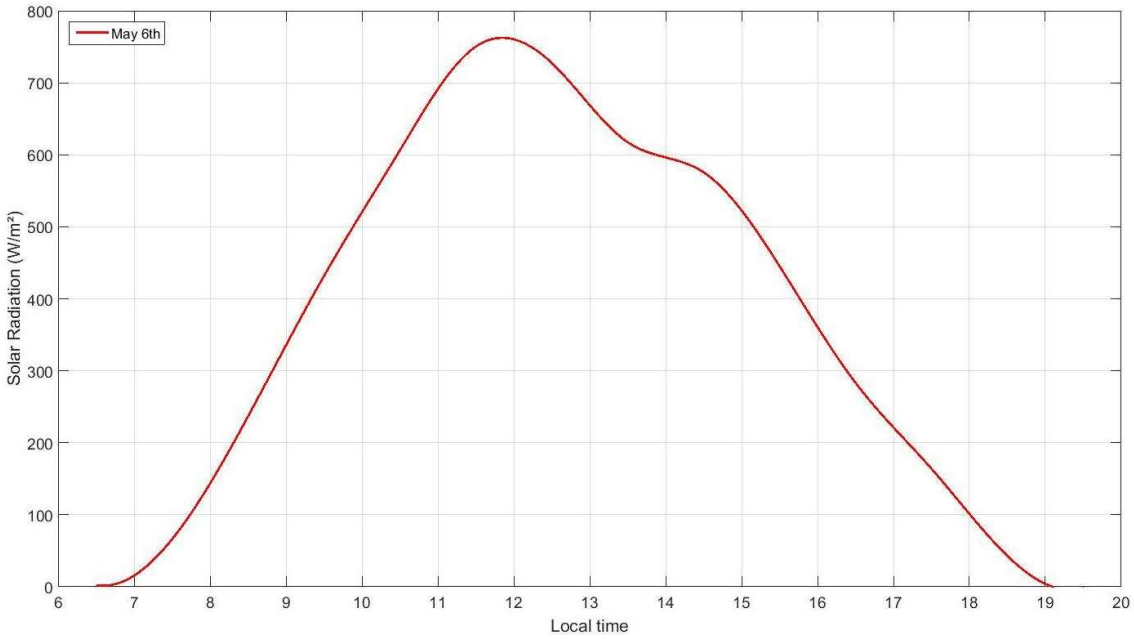

Fig. 6 Solar radiation intensity corresponding to the representative day of test with gold nanofluids (May 6th)

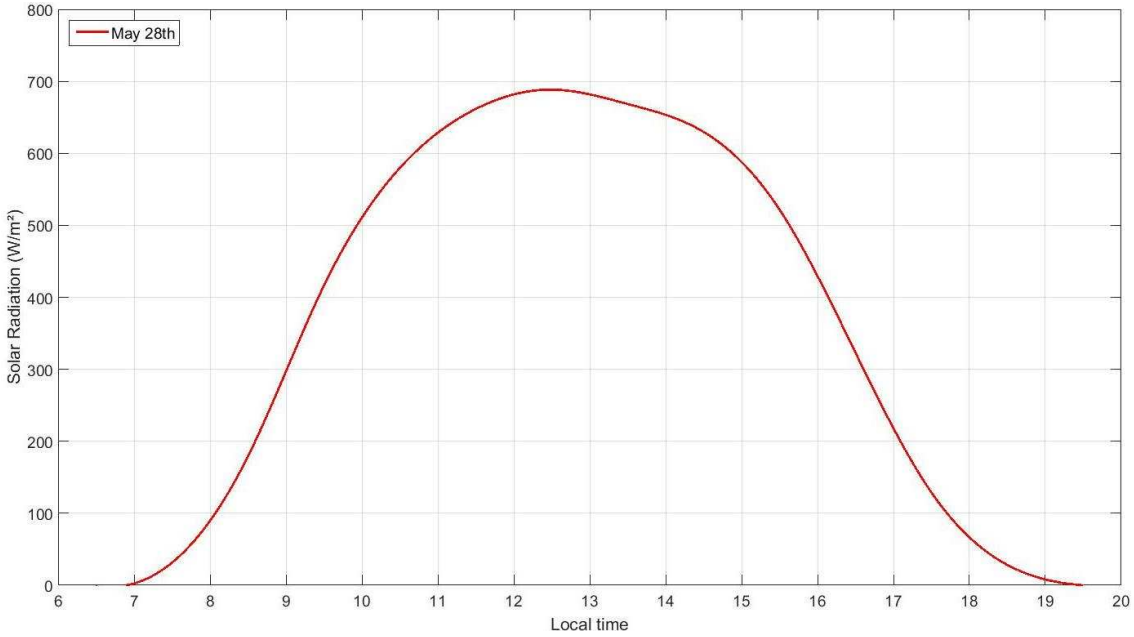

Fig. 7 Solar radiation intensity corresponding to the representative day of test with MWCNT nanofluids (May 28th)

3 Calculation

The photothermal conversion performance analysis was evaluated based on three parameters, the specific absorption rate, the stored energy ratio and the total energy absorbed in the heating phase.

The specific absorption rate describes the particle's capability in absorbing energy per unit mass and can be calculated as:

$$SAR = \frac{(m_{bf}c_{bf} + m_{np}c_{np})\Delta T_{nf} - m_{bf}c_{bf}\Delta T_{bf}}{1000 m_{np}\Delta t} \quad (1)$$

Where SAR is the nanoparticle's specific absorption rate (kW/g), m represents the mass (g), c the specific heat (kJ/g^{o}C), T the temperature and t the time (s). The subscripts bf, np and nf represents the base fluid, nanoparticle and nanofluid, respectively.

As $m_{np}c_{np} \ll m_{bf}c_{bf}$, then, the equation can be simplified as:

$$SAR = \frac{m_{bf}c_{bf}}{1000 m_{np}}\left(\frac{\Delta T_{nf}}{\Delta t} - \frac{\Delta T_{bf}}{\Delta t}\right) \quad (2)$$

The stored energy ratio (SER) provides information about the "extra" energy absorbed by the nanofluid due to the presence of the nanoparticles. Thus, the "SER" can be calculated as the ratio between the heat stored by the nanofluid and its respective base fluid, as follows:

$$SER = \frac{Q_{nf}(t)}{Q_{bf}(t)} = \frac{(m_{bf}c_{bf} + m_{np}c_{np})(T_{nf}(t) - T_{nf}(0))}{m_{bf}c_{bf}(T_{bf}(t) - T_{bf}(0))} \quad (3)$$

And the equation can be simplified by the same principle as the SAR, and then:

$$SER = \frac{(T_{nf}(t) - T_{nf}(0))}{(T_{bf}(t) - T_{bf}(0))} \quad (4)$$

The total energy stored by the fluids studied during the heating phase – the time between the sunrise and the noontime - is proportional to the maximum temperature variation experienced by each fluid during the test period, being calculated as:

$$E_{total} = m_f \, c_f \, (T_{max} - T_{min}) \quad (5)$$

4 Results and Discussion

The experimental results are presented separated by nanofluid type and a summarized discussion concerning to both nanofluids is made at the end of this section.

4.1 Gold nanofluids

Fig. 8 through Fig. 10 present the temperature profiles in three test days with gold nanofluids. It is notable that during the first 5000 seconds of each test, especially the one shown in Fig. 10, the temperature profiles resemble an exponential curve, and then present a parabolic behavior. The first day of tests (May 6th), illustrated by Fig. 8, showed the most promising results of nanofluids in comparison with the base fluid, where significant temperature increase was seen at concentrations up to 0.003%, and a similar behavior of the two nanofluids with higher concentrations is observable (0.003% and 0.004%).

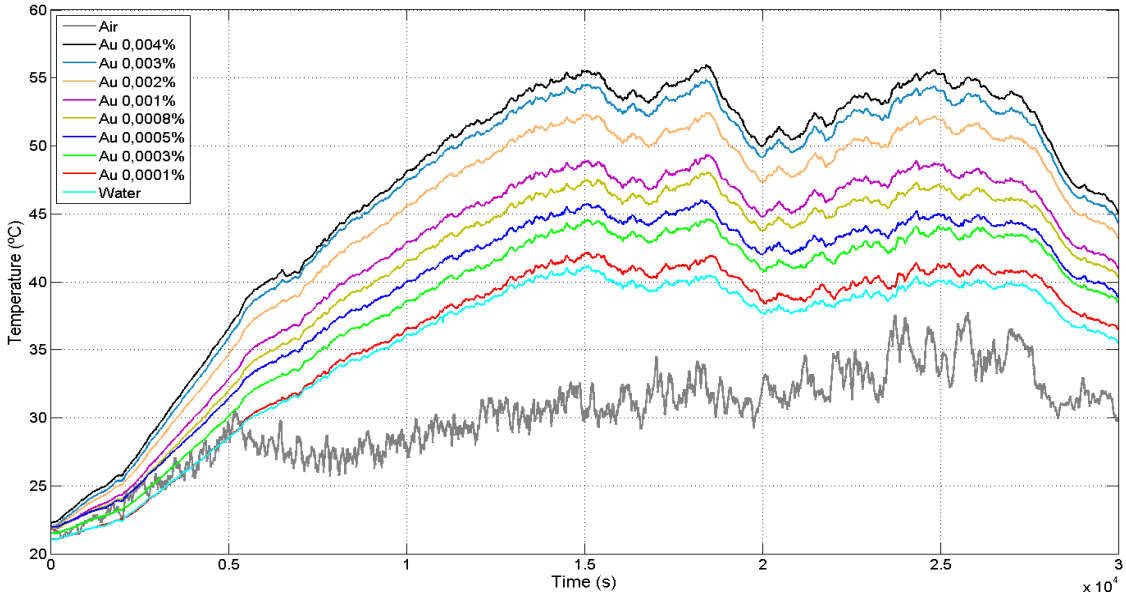

Fig. 8 Temperature profiles of gold nanofluids and base fluid tested on May 6th (first day of tests).

It was observed that from the third test day, represented by Fig. 9, the results were different from the expected augmentation of the temperature with volumetric concentration (as occurred in the first test day, Fig. 8). Two overlaps can be seen in the graph: between the temperature profiles of nanofluid with the lowest concentration (Φv = 0.0001%) and water and between the 0.0003% and 0.0005% nanofluids concentrations.

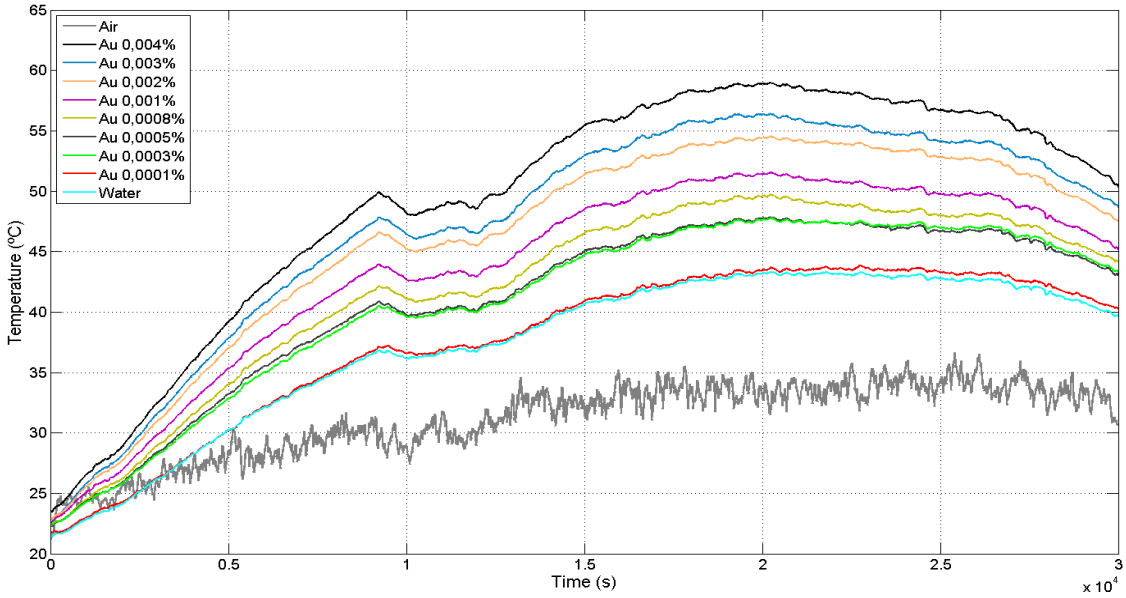

Fig. 9 Temperature profiles of gold nanofluids in water and base fluid tested on 8th May (third day of tests).

At the fifth test day, as can be seen in Fig. 10 and Fig. 11, the nanofluids showed remarkable evidence of degradation such as sample color change, the similarity between the samples temperature profiles and the surprising behavior of the nanofluid with the lowest concentration (Φv = 0.0001%), that showed lower temperatures than the water sample. This behavior can be explained by the visible agglomeration and adhesion of particles on the container (Fig. 12), which creates a layer of gold particles on the surface

of the acrylic, which may reduce the absorption of the solar light. The phenomenon of photothermal conversion ceases to be volumetric and becomes superficial, concentrated in the outermost layer of the container, where the greatest heat loss to the environment occurs through convection.

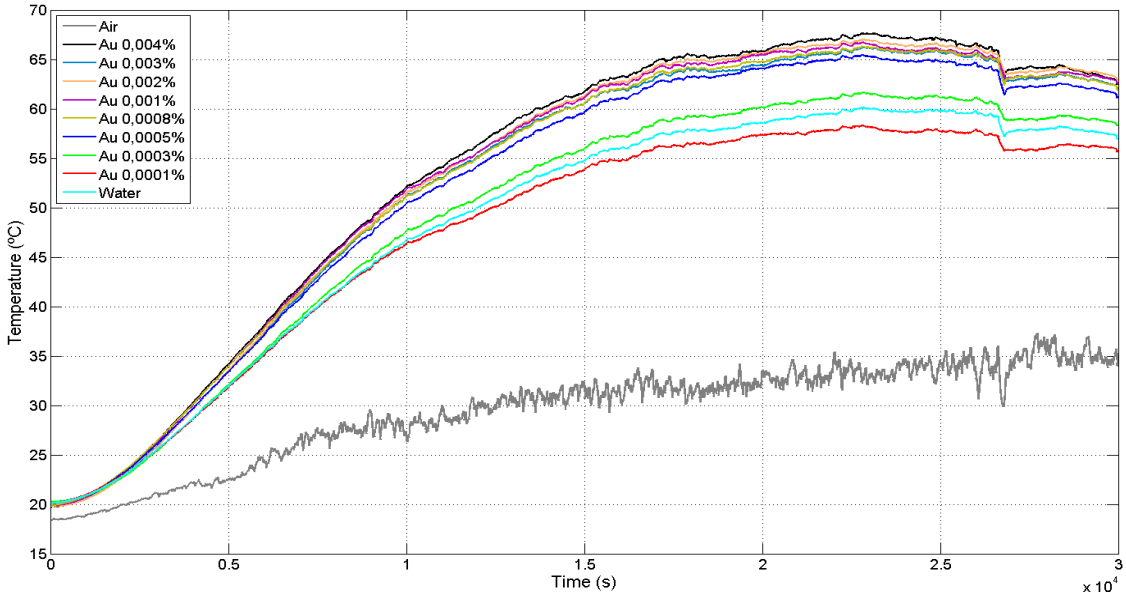

Fig. 10 Temperature profiles of gold nanofluids in water and base fluid tested on 22th May (fifth day of tests)

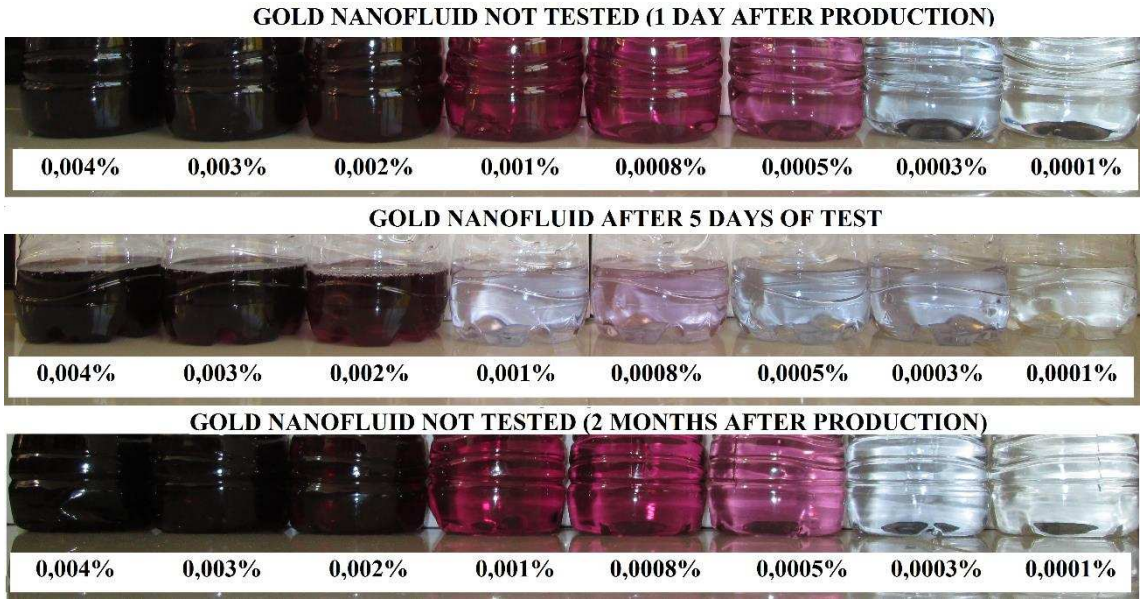

Fig. 11 Comparative photos of the unused samples, one day and two months after the synthesis, and after five days of testing.

Fig. 12 Images of the particle agglomerations (a) at the bottom and (b) on the surface of the container.

Fig. 13 shows the values of SER for the gold nanofluids in water for the different volumetric concentrations tested on May 6th. It is possible to observe that the SER increased with the addition of nanoparticles to the base fluid, with the highest concentration (Φv =0.004%) presenting the best results and the lowest concentration (Φv =0.0001%) the less expressive results, with a stored energy similar to that of the water (SER≈1).

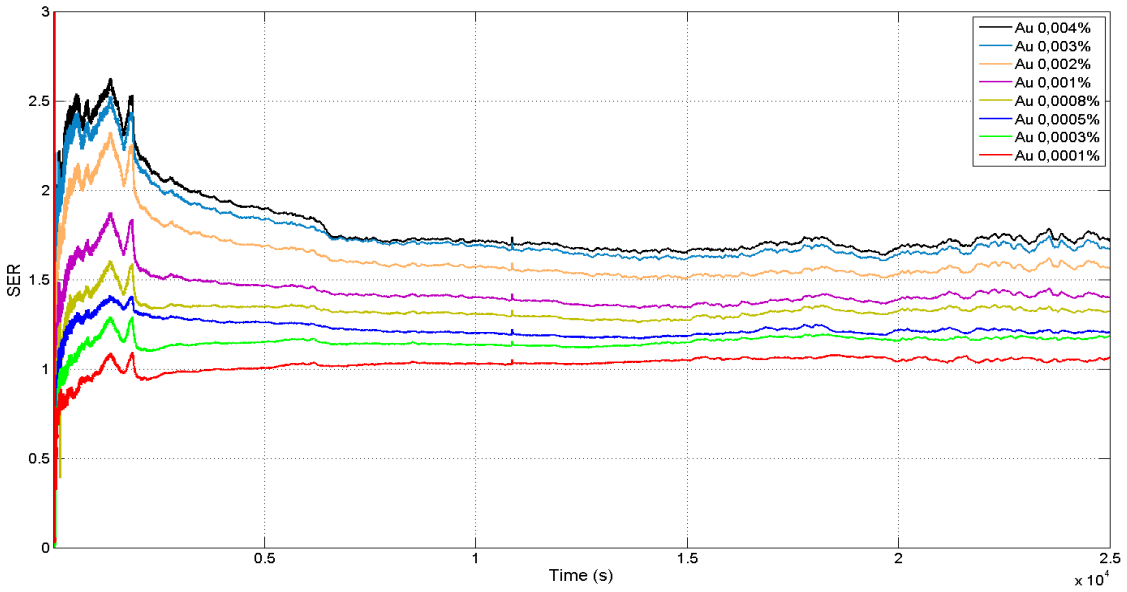

Fig. 13 Stored Energy Ratio (SER) for gold nanofluids, (tested on May 6th).

Fig. 14 graphically presents the values showed in the Table 5 for the total energy stored during the heating phase of the fluids as a function of the volumetric concentration, where the interception at the y axis refers to water. It is observed an approximately parabolic behavior for this parameter, being almost linear for concentrations up to 0.0001%.

Table 5 - Maximum and minimum temperatures, maximum temperature variation and total energy stored for gold nanofluids (tested on May 6th).

ϕ_v (%)	T_{min} (ºC)	T_{max} (ºC)	ΔT_{max} (ºC)	E_{Total} (kJ)
0.004	22.3	55.4	33.1	13.844
0.003	22.0	54.4	32.4	13.525
0.002	22.0	52.1	30.2	12.611
0.001	21.8	48.8	27.0	11.272
0.0008	21.9	47.3	25.4	10.614
0.0005	21.9	45.5	23.6	9.862
0.0003	21.5	44.3	22.8	9.548
0.0001	21.0	42.0	20.9	8.752
0 (Water)	21.0	41.1	20.0	8.380

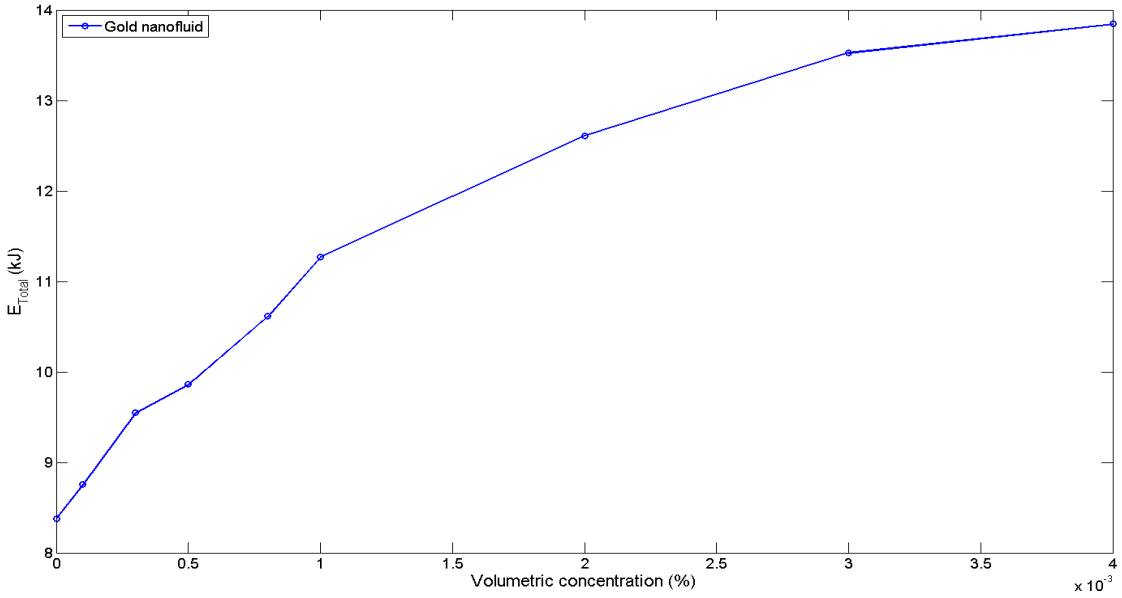

Fig.14 Total energy stored in the heating phase in function of the volumetric concentration of gold nanoparticles (tested on May 6th).

Fig. 15 presents the maximum SAR values for each gold nanofluid volumetric concentrations tested on May 6th. The lowest nanofluid concentration (Φv =0.0001%) showed the highest SAR value and the highest concentration (Φv =0.004%), the lowest value. The observed behavior implies that the difference between the temperature variation rate of nanofluids and water hasn't increased at the same ratio as the nanoparticle concentration and that the photothermal conversion capability per nanoparticle decreases at higher particle loadings.

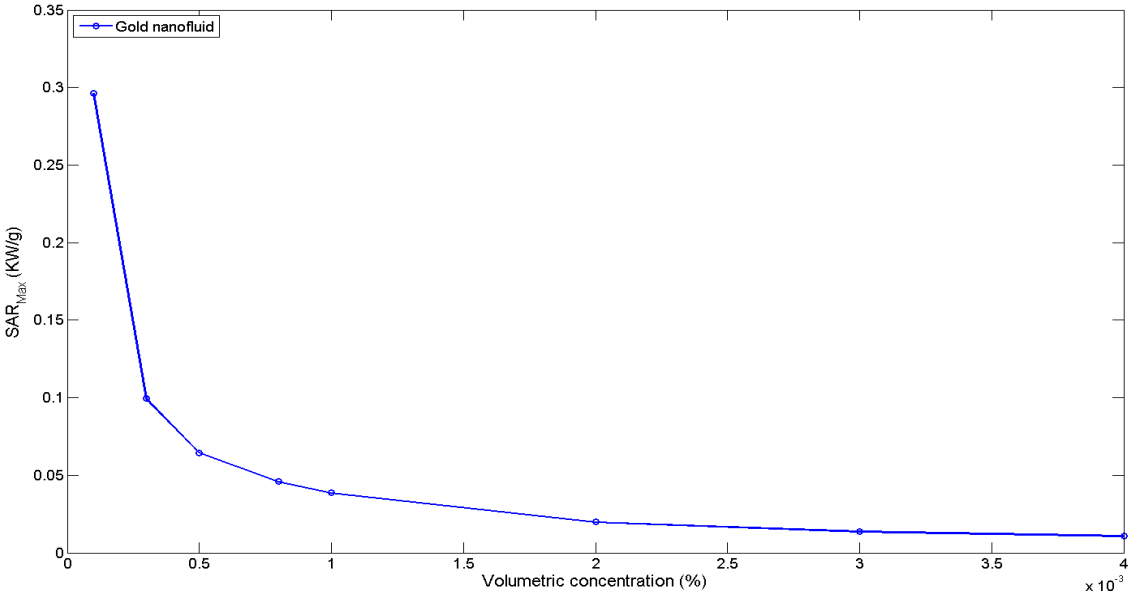

Fig. 15 Specific Absorption Rate (SAR): maximum values for each volumetric concentration of gold nanofluids in water (tested on May 6th).

The observed behavior of decrease of the SAR with the increase of the concentration of nanoparticles in the base fluid could be explained by two hypotheses. The first one is based on the formation of agglomerations at higher particle loadings, which causes a non-linear increase in the amount of particles in the fluid. The agglomerations do not behave in the same way as isolated nanoparticles and have reduced specific surface area. The second is based on the increase in the amount of nanoparticles close to the collector surface, which could cause a decrease in the intensity of incident radiation on the fluid at different depths. It can also result in an increase in heat losses, since the phenomenon happens primarily on the area near the acrylic's surface, where the highest heat losses to the ambient occurs.

4.2 MWCNT nanofluids

All testing days using MWCNT/water nanofluids showed similar results then, the temperature profiles and the parameters SER, SAR and total energy storage are represented by one of the test day, the May 28th, a partially cloudy day, with a weather condition similar to that of gold/water nanofluids test made on May 6th.

Representing the temperature behavior, the temperature profiles for the fluids tested on May 28 are presented in Fig. 16 and Fig. 17. For better visualization of the data, each test day was separated into two ranges of volumetric concentration, one ranging from 0.0001% to 0.002% and other from 0.002% to 0.03%.

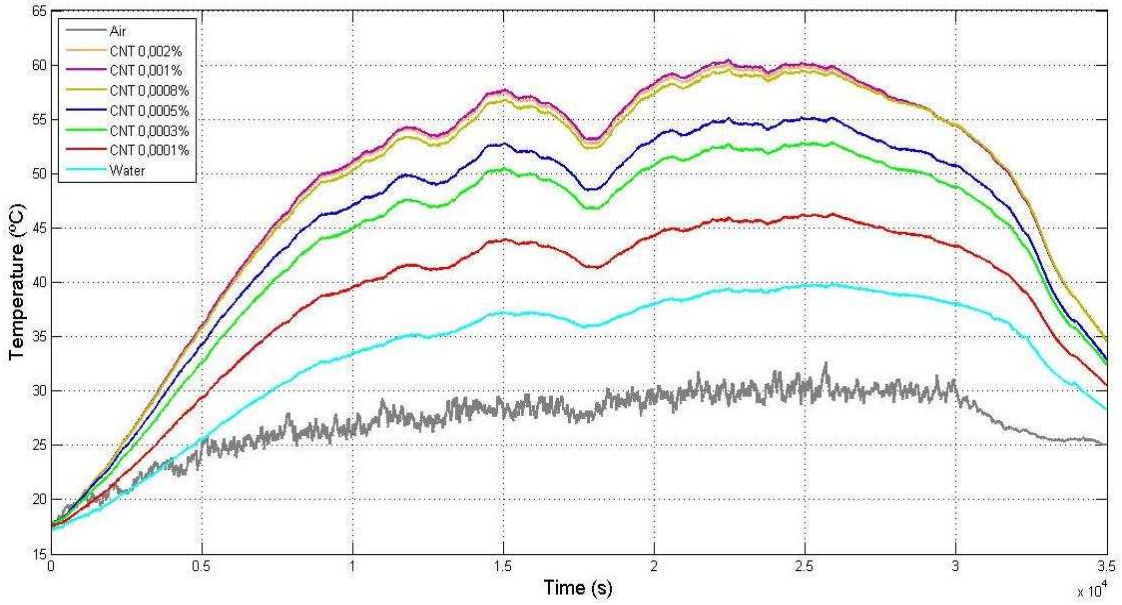

Fig. 16 Temperature profiles of lower nanoparticle concentrations of MWCNT/water nanofluids and base fluid tested on 28th May (partly cloudy test day).

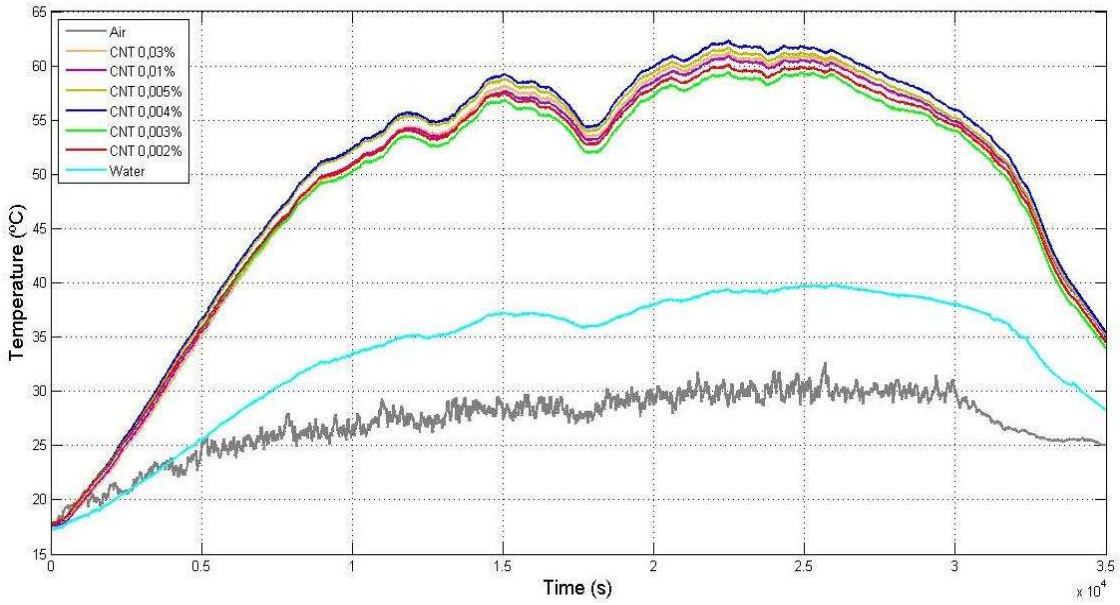

Fig. 17 Temperature profiles of higher nanoparticle concentrations of MWCNT/water nanofluids and base fluid tested on 28th May (partly cloudy test day).

It is noted that the addition of nanoparticles to the base fluid produces effects of increasing the maximum temperature reached and heating rate for the nanofluids studied, however, this tendency is just noted up to the 0.001% volumetric concentration. There is no significant variation for the 0.002% sample and higher concentrations. The indistinguishable behavior presented by the higher concentrations (0.002% to 0.03%) in Fig. 17 suggests that the addition of nanoparticles to the water has a limit, a concentration from which no significant gains in photothermal conversion are observed, that makes the application of higher MWCNT concentrations uneconomic. It is possible to infer that, for the MWCNT/water nanofluid studied, the limit volumetric concentration would be around 0.001%.

The absence of clouds during a test day has not changed the general trend seen in Fig. 16 an Fig. 17, just provided more stable increases to the temperature profiles, without intermittent temperature declines and maximum values slightly higher than that of the days with clouds (see table 6 for comparative data).

It is observed in Fig. 18 that the SER increases with the addition of nanoparticles up to the concentration of 0.001%, not presenting values that could suggest a specific tendency at higher concentrations (see Table 7 for complementary information). The result obtained for the 0.002% volumetric concentration reaffirms the existence of a limit particle loading for the base fluid used, since the addition of nanoparticles above the 0.001% concentration did not provide an increase in the stored energy ratio.

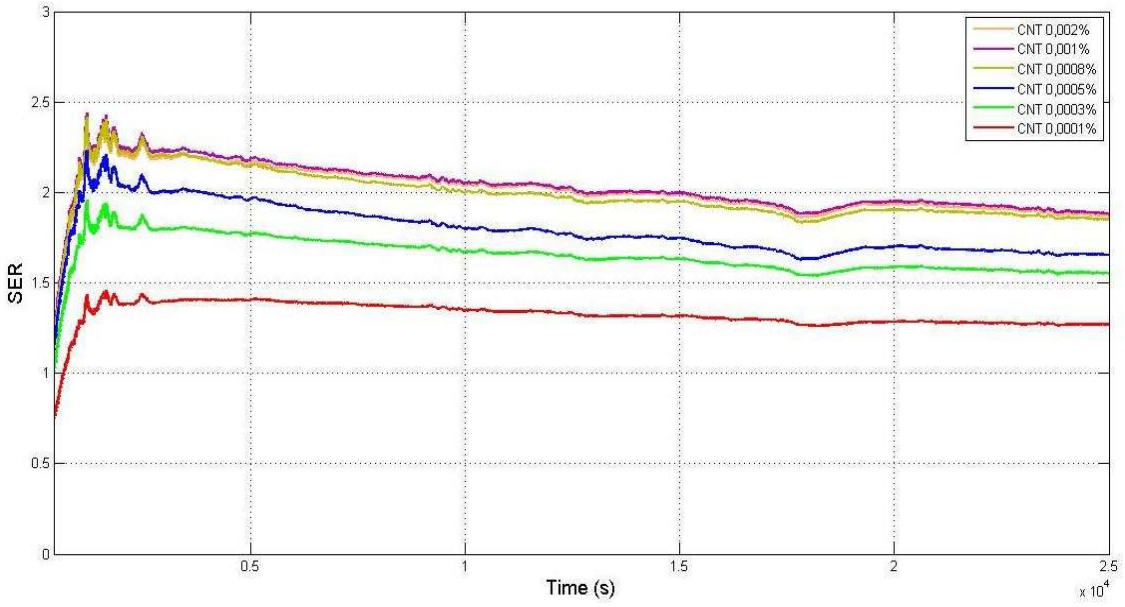

Fig. 18 Stored Energy Ratio (SER) of lower nanoparticle concentrations of MWCNT/water nanofluids tested on 28th May (partly cloudy test day).

Table 6 presents some comparative data results for a partially cloudy weather condition and a sunny day test. It can be seen the differentiation for the values of the maximum temperature (T_{max}), maximum temperature variation (ΔT_{max}) and the total energy stored during heating phase (E_{Total}) for MWCNT/water nanofluids and its base fluid tested under partly cloudy condition, on 28th May, and on a sunny day, the 30th May. It is observed that all the nanofluids showed superior performance compared to water.

For the partly cloudy test day, the lowest increment was observed in the concentration of 0.0001%, with a result 27% higher than the base fluid. For the 0.001% concentration, 92% higher gain was obtained while the 0.004% sample presented the best result with a total absorbed energy 100% higher than that obtained by the base fluid.

Table 6 - Maximum and minimum temperatures, maximum temperature variation and total energy stored for MWCNT/water nanofluids for two different weather conditions.

ϕv (%)	Partly cloudy test day (28th May)			Sunny test day (30th May)		
	Tmax (ºC)	ΔTmax (ºC)	ETotal (kJ)	Tmax (ºC)	ΔTmax (ºC)	ETotal (kJ)
0.03	61.0	43.5	18.187	65.2	47.6	19.886
0.01	60.6	43.0	17.981	63.2	45.3	18.931
0.005	61.4	43.7	18.275	64.0	46.0	19.211
0.004	62.0	44.4	18.543	64.4	46.6	19.488
0.003	59.1	41.4	17.292	63.7	45.6	19.069
0.002	59.9	42.1	17.583	62.8	44.7	18.664
0.001	60.2	42.4	17.714	63.3	45.1	18.857
0.0008	59.3	41.5	17.335	61.8	43.5	18.168
0.0005	54.8	36.9	15.437	59.6	41.2	17.202
0.0003	52.5	34.6	14.463	56.0	37.6	15.721
0.0001	45.8	28.1	11.761	48.8	30.7	12.851
0(Water)	39.3	22.0	9.209	40.2	22.8	9.527

It can be seen from Fig. 19 that for concentrations up to 0.001%, the increase in nanoparticle concentration causes an approximately linear increase in the total energy stored, without expressive increments above the 0.001% nanoparticle concentration. It is also noted that, although the maximum gain point occurs at the 0.004% concentration, the difference between the best result and that obtained by the 0.001% concentration is small (about 4%) and the nanoparticle quantity used is much higher (four times higher), which would not justify the expenditure needed for the application of concentrations above 0.001%.

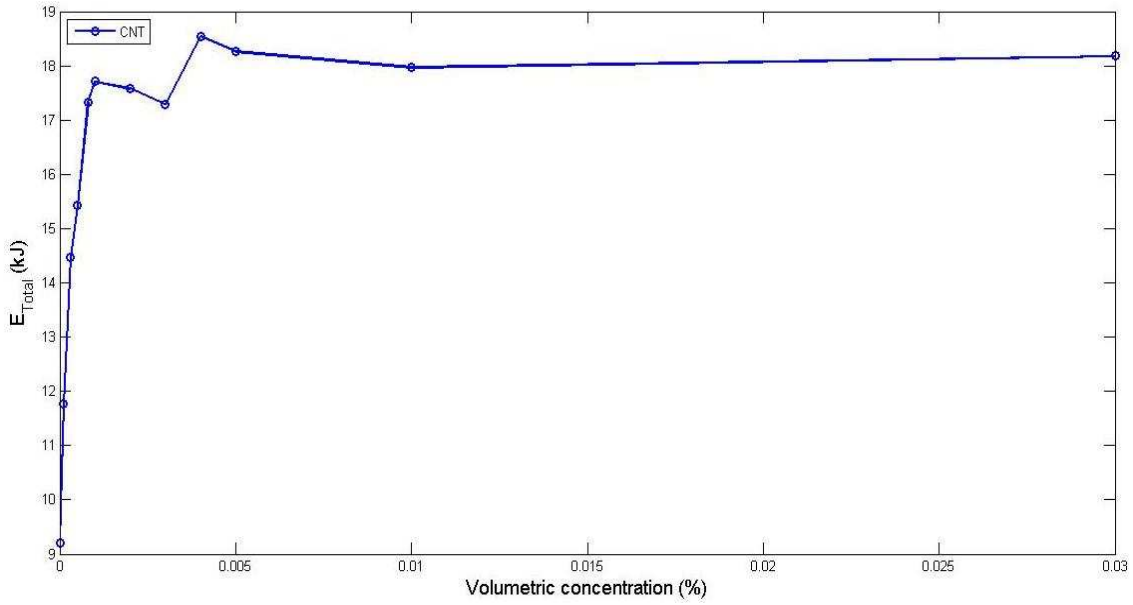

Fig. 19 Total energy stored in the heating phase in function of the MWCNT volumetric concentration (tested on May 28th, partly cloudy test day).

It is observed from Fig. 20 that as seen for gold nanofluids, the value of SAR decreases with increasing concentration of nanoparticles, with the 0.0001% and 0.03% samples presenting the best and worst results, respectively. It is also noted that the reduction in SAR value reaches a stabilization at higher nanoparticle concentrations, values greater than 0.002% in volume, reaffirming the behavior presented by the total energy stored, which has previously indicated the 0,001% sample as a limit nanoparticle concentration for the studied MWCNT/water nanofluid.

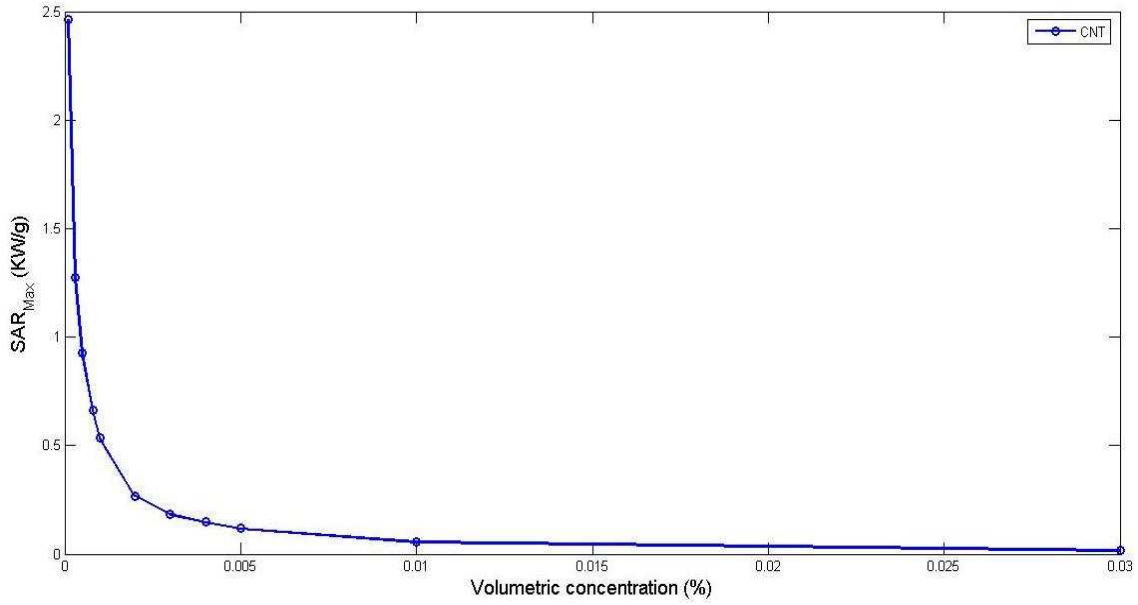

Fig. 20 Maximum values of Specific Absorption Rate (SAR) against MWCNT/water volumetric concentrations (tested on 28th May, partly cloudy test day).

4.3 Discussion

Table 7 presents comparative results for maximum SER and SAR values and total energy stored in the heating phase for gold and MWCNT nanofluids under partly cloudy weather condition. It is noted that, unlike the observed value of SER of the lowest concentration of gold nanofluids (0.0001% by volume, SER≈1.1), the calculated value for the corresponding MWCNT/water sample presented more expressive results, around 1.4, however, the nanoparticles addition above the 0.002% volumetric concentration leaded the gold nanofluids samples to better results. Moreover, the total energy absorbed during the heating phase and the SAR values obtained for all MWCNT/water concentrations presented better results compared to those obtained by gold/water samples.

Table 7 – Comparative results for maximum SER and SAR values and total energy stored in the heating phase for gold and MWCNT nanofluids tested under partly cloudy weather condition.

ϕv (%)	SER_{max}		E_{Total} (kJ)		SAR_{max} (kW/g)	
	Gold	MWCNT	Gold	MWCNT	Gold	MWCNT
0.03	-	2.12	-	18.187	-	0.018
0.01	-	2.17	-	17.981	-	0.059
0.005	-	2.30	-	18.275	-	0.119
0.004	2.62	2.35	13.844	18.543	0.011	0.147
0.003	2.52	2.23	13.525	17.292	0.014	0.184
0.002	2.32	2.22	12.611	17.583	0.020	0.269
0.001	1.87	2.25	11.272	17.714	0.039	0.535
0.0008	1.60	2.22	10.614	17.335	0.046	0.660
0.0005	1.41	2.02	9.862	15.437	0.064	0.929
0.0003	1.29	1.81	9.548	14.463	0.100	1.274
0.0001	1.09	1.41	8.752	11.761	0.296	2.464
0(Water)	-	-	8.380	9.209	-	-

It is important to highlight that the SAR parameter (Eq. 1 and 2) was calculated considering the mass of nanoparticles used in the samples production to make clearly the relation between the economical expenditure with the materials used in each nanofluid and the respective photothermal conversion results obtained. However, to understand the influence of the volume of nanoparticles dispersed in the base fluid on the solar radiation absorption, we could define the volumetric specific absorption rate (VSAR) as follows:

$$\mathrm{VSAR} = \mathrm{SAR} \times \rho_{np} \quad (6)$$

Where SAR is the specific absorption rate calculated as Eq. (2) and ρ_{np} is the density of the nanoparticle material.

It can be observed from the nanofluids maximum VSAR values presented in Fig. 21 that, although most of MWCNT samples obtained slightly better results, the

nanoparticle material is not the most influential factor in the photothermal conversion results obtained, since VSAR values were similar for gold nanoparticles and MWCNT, despite the great difference in the nature of the studied materials.

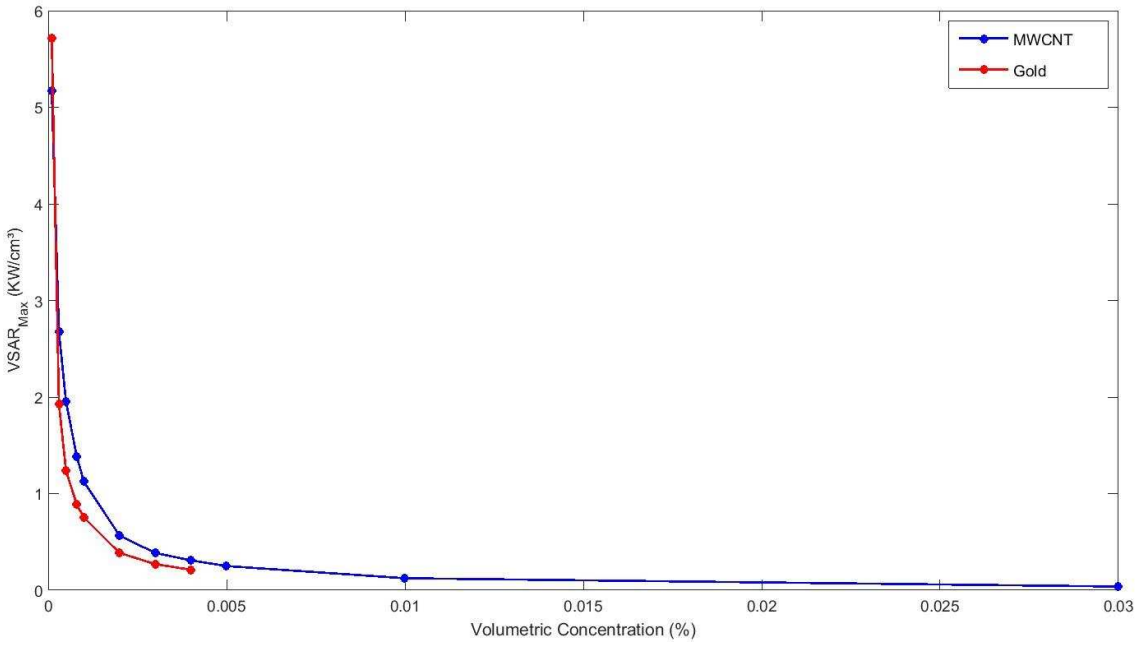

Fig. 21 Maximum values of Volumetric Specific Absorption Rate (VSAR) for gold and MWCNT nanofluids tested under partly cloudy weather condition.

5 Conclusions

This work experimentally investigated the effect of nanoparticle volumetric fraction on the photothermal conversion characteristics of MWCNT/water and Gold/water nanofluids under realistic solar exposure conditions. The results and their analysis leaded to the following conclusions:

- The temperature variation of the samples along the test day changed from an approximately exponential growth at the first 5000 seconds of test to a parabola-like curve for the rest of solar exposure time.

- SAR showed a clear downward trend with increasing the nanoparticle volumetric fraction. The SAR presented an exponential decay with increasing sample's volumetric concentration, with no further increase for concentrations higher than 0.001% and 0.002% for gold/water and MWCNT/water nanofluids, respectively.
- The addition of nanoparticles to the base fluid caused an increase in the total energy stored by the fluids during the heating period, showing an approximately linear relationship between stored energy and nanoparticle volume for concentrations between 0.0001% and 0.001% for both nanofluids.
- SER showed maximum values at the beginning of the tests. SER increased with the addition of nanoparticles for all concentrations of gold nanofluids (reaching the maximum at the 0.004% concentration) and, in the case of MWCNT nanofluids, SER increased with concentration between 0.0001% and 0.001%, not reaching better results with extra nanoparticle addition.
- The combined analysis of the studied parameters corroborates the existence of an "optimal" volumetric concentration, above which further nanoparticle addition becomes indifferent or infeasible. The optimal volumetric concentrations for the nanofluids under consideration were found to be 0.002% for the gold nanoparticles and 0.001% for the MWCNT samples.

Despite the initial expectations of superior results promoted by the LSPR phenomenon for the plasmonic gold nanofluid, the economic and practical factors associated with its use, such as the high production cost of gold nanoparticles and the visible degradation of the samples after prolonged exposure to solar radiation suggest that the MWCNT/water nanofluids having better photothermal results and long term stability

would be more feasible for photothermal conversion applications for its lower production cost under similar conditions to those used in this work.

Acknowledgements

This work was supported by CAPES, CNPq and FAPEMIG.

References

[1] J. E. MINARDI, H. N. CHUANG, Performance of a “black” liquid flat-plate solar collector, Solar Energy. 17-3 (1975) 179-183.

[2] J. R. SWIDER, V. A. HACKLEY, J. WINTER, Characterization of Chinese ink in size and surface, Journal of Cultural Heritage. 4 (2003) 175–186.

[3] N. ARAI, Y. ITAYA, M. HASATANI, Development of a "volume heat-trap" type solar collector using a fine-particle semitransparent liquid suspension (fpss) as a heat vehicle and heat storage medium, Solar Energy. 32 (1984) 49-56.

[4] S. U. S. CHOI, J. A. EASTMAN, Enhancing thermal conductivity of fluids with nanoparticles, ASMEFED. 231 (1995) 99-103.

[5] D. WEN, G. LIN, S. VAFAEI, K. ZHANG, Review of nanofluids for heat transfer applications, Particuology. 7 (2009) 93-160.

[6] T. OTANICAR, P. E. PHELAN, R. S. PRASHER, G. ROSENGARTEN, R. A. TAYLOR, Nanofluid-based direct absorption solar collector, Journal of Renewable Sustainable Energy. 2(3) (2010) id 033102.

[7] R. A. TAYLOR, P. E. PHELAN, T. P. OTANICAR, C. A. WALKER, M. NGUYEN, S. TRIMBLE, R. PRASHER, Applicability of nanofluids in high flux solar collectors, Journal of Renewable and Sustainable Energy. 3 (2011a) id 023104.

[8] R. A. TAYLOR, P. E. PHELAN, T. P. OTANICAR, R. ADRIAN, R. PRASHER, Nanofluid optical property characterization: towards efficient direct absorption solar collectors, Nanoscale Research Letters. 6 (2011b) 225.

[9] Y. HE, S. WANG, J. MA, F. TIAN, Y. REN, Experimental study on the light-heat conversion characteristics of nanofluids, Nanoscience and Nanotechnology Letters. 3 (2011) 494–496.

[10] A. LENERT, E. N. WANG, Optimization of nanofluid volumetric receivers for solar thermal energy conversion, Solar Energy. 86 (2012) 253–265.

[11] T. YOUSEFI, F. VEYSI, E. SHOJAEIZADEH, S. ZINADINI, An experimental investigation on the effect of Al2O3-H2O nanofluid on the efficiency of flat-plate solar collectors, Renewable Energy. 39 (2012a) 293-298.

[12] T. YOUSEFI, E. SHOJAEIZADEH, F. VEYSI, S. ZINADINI, An experimental investigation on the effect of pH variation of MWCNT–H2O nanofluid on the efficiency of a flat-plate solar collector, Solar Energy. 86 (2012b) 771–779.

[13] T. YOUSEFI, F. VEYSI, E. SHOJAEIZADEH, S. ZINADINI, An experimental investigation on the effect of MWCNT–H2O nanofluid on the efficiency of flat-plate solar collector, Experimental Thermal and Fluid Science. 39 (2012c) 207–212.

[14] V. KHULLAR, H. TYAGI, P. E. PHELAN, T. P. OTANICAR, H. SINGH, R. A. TAYLOR, Solar energy harvesting using nanofluids-based concentrating solar collector, In: International Conference on Micro/Nanoscale Heat and Mass Transfer 3, Atlanta, Georgia, USA. ASME Proceedings - MNHMT2012 (2012) 259-267.

[15] Q. HE, S. WANGA, S. ZENG, Z. ZHENG, Experimental investigation on photothermal properties of nanofluids for direct absorption solar thermal energy systems, Energy Conversion and Management. 73 (2013) 150–157.

[16] M. T. JAMAL-ABAD, A. ZAMZAMIAN, E. IMANI, M. MANSOURI, Experimental Study of the Performance of a Flat-Plate Collector Using Cu–Water Nanofluid, Journal of Thermophysics and Heat Transfer. 27-4 (2013) 756-760.

[17] Z. LIU, R. HUA, L. LU, F. ZHAO, H. XIAO, Thermal performance of an open thermosyphon using nanofluid for evacuated tubular high temperature air solar collector, Energy Conversion and Management. 73 (2013) 135–143.

[18] Q. HE, S. ZHENG, S. WANG, Experimental investigation on the efficiency of flat-plate solar collectors with nanofluids, Applied Thermal Engineering. 88 (2014) 165–171.

[19] N. HORDY, D. RABILLOUD, J. L. MEUNIER, S. COULOMBE, High temperature and long-term stability of carbon nanotube nanofluids for direct absorption solar thermal collectors, Solar Energy. 105 (2014) 82–90.

[20] E. P. BANDARRA FILHO, O. S. H. MENDOZA, C. L. L. BEICKER, A. MENEZES, D. WEN, Experimental investigation of a silver nanoparticle-based direct absorption solar thermal system, Energy Conversion and Management. 84 (2014) 261–267.

[21] M. KARAMI, M. A. AKHAVAN-BAHABADI, S. DELFANI, A. GHOZATLOO, A new application of carbon nanotubes nanofluid as working fluid of low-temperature direct absorption solar collector, Solar Energy Materials & Solar Cells. 121 (2014) 114–118.

[22] H. ZHANG, H. CHEN, X. DUA, D. WEN, Photothermal conversion characteristics of gold nanoparticle dispersions, Solar Energy. 100 (2014) 141–147.

[23] H. K. GUPTA, G. D. AGRAWAL, J. MATHUR, An experimental investigation of a low temperature Al2O3-H2O nanofluid based direct absorption solar collector, Solar Energy. 118 (2015) 390-396.

[24] M. KARAMI, M. A. AKHAVAN-BAHABADI, S. DELFANI, M. RAISEE, Experimental investigation of CuO nanofluid based direct absorption solar collector for residential applications, Renewable and Sustainable Energy Reviews. 52 (2015) 793-801.

[25] M. A. SABIHA, R. SAIDUR, S. HASSANI, Z. SAID, S. MEKHILEF, Energy performance of an evacuated tube solar collector using single walled carbon nanotubes nanofluids, Energy Conversion and Management. 105 (2015) 1377-1388.

[26] S. SALAVATI MEIBODI, H. NIAZMAND, O. MAHIAN, S. WONGWISES, Experimental investigation on the thermal efficiency and performance characteristics of a flat plate solar collector using SiO2/EG– water nanofluids, International Communications in Heat and Mass Transfer. 65 (2015) 71-75.

[27] Y. TONG, J. KIM, H. CHO, Effects of thermal performance of enclosed-type evacuated U-tube solar collector with multi-walled carbon nanotube/water nanofluid, Renewable Energy. 83 (2015) 463-473.

[28] S. DELFANI, M. KARAMI, M. A. AKHAVAN-BEHABADI, Performance characteristics of a residential-type direct absorption solar collector using MWCNT nanofluid, Renewable Energy. 87 (2016) 754-764.

[29] M. VAKILI, S. M. HOSSEINALIPOUR, S. DELFANI, S. KHOSROJERDI, M. KARAMI, Experimental investigation of graphene nanoplatelets nanofluid-based volumetric solar collector for domestic hot water systems, Solar Energy. 131 (2016) 119-130.

[30] S. K. VERMA, A. K. TIWARI, D. S. CHAUHAN, Performance augmentation in flat plate solar collector using MgO/water nanofluid, Energy Conversion and Management 124 (2016) 607-617.

[31] D. A. VINCELY, E. NATARAJAN, Experimental investigation of the solar FPC performance using graphene oxide nanofluid under forced circulation, Energy Conversion and Management. 117 (2016) 1–11.

[32] J. JEON, S. PARK, B. J. LEE, Analysis on the performance of a flat-plate volumetric solar collector using blended plasmonic nanofluid, Solar Energy. 132 (2016) 247-256.

[33] M. CHEN, Y. HE, J. ZHU, D. R. KIM, Enhancement of photo-thermal conversion using gold nanofluids with different particle sizes, Energy Conversion and Management. 112 (2016) 21–30.

[34] M. AMJAD, G. RAZA, Y. XIN, S. PERVAIZ, J. XU, X. DU, D. WEN, Volumetric solar heating and steam generation via gold nanofluids, Applied Energy. 206 (2017) 393-400

[35] Y. FU, T. MEI, G. WANG, A. GUO, G. DAI, S. WANG, J. WANG, J. LI, X. WANG, Investigation on enhancing effects of Au nanoparticles on solar steam generation in graphene oxide nanofluids, Applied Thermal Engineering. 114 (2017) 961–968.

[36] B. A. J. ROSE, H. SINGH, N. VERMA, S. TASSOU, S. SURESH, N. ANANTHARAMAN, D. MARIOTTI, P. MAGUIRE, Investigations into nanofluids as direct solar radiation collectors, Solar Energy. 147 (2017) 426-431.

[37] S. IRANMANESH, H. C. ONG, B. C. ANG, E. SADEGHINEZHAD, A. ESMAEILZADEH, M. MEHRALI, Thermal performance enhancement of an evacuated tube solar collector using graphene nanoplatelets nanofluid, Journal of Cleaner Production. 162 (2017) 121-129.

[38] M. CHEN, Y. HE, J. HUANG, J. ZHU, Investigation into Au nanofluids for solar photothermal conversion, International Journal of Heat and Mass Transfer. 108 (2017) 1894–1900.

[39] H. WANG, W. YANG, L. CHENG, C. GUAN, H. YAN, Chinese ink: High performance nanofluids for solar energy, Solar Energy Materials and Solar Cells. 176 (2018) 374–380.

[40] I.M. MAHBUBUL, M. M. A. KHAN, N. I. IBRAHIM, H. M. ALI, F. A. AL-SULAIMAN, R. SAIDUR, Carbon nanotube nanofluid in enhancing the efficiency of evacuated tube solar collector, Renewable Energy. 121 (2018) 36-44.

[41] H. DUAN, L. TANG, Y. ZHENG, C. XU, Effect of plasmonic nanoshell-based nanofluid on efficiency of direct solar thermal collector, Applied Thermal Engineering. 133 (2018) 188–193.

[42] X. LIU, X. WANG, J. HUANG, G. CHENG, Y. HE, Volumetric solar steam generation enhanced by reduced graphene oxide nanofluid, Applied Energy. 220 (2018) 302–312.

[43] M. DU, G. H. TANG, Plasmonic nanofluids based on gold nanorods/nanoellipsoids/nanosheets for solar energy harvesting, Solar Energy. 137 (2016) 393–400

[44] R. B. ABERNETHY, J. W. THOMPSON, Uncertainties in gas turbine measurements, AEDC Technical Library, Tennessee, USA, 1973.

[45] ABNT, ABNT/NBR 15569-2008, Solar water heating systems in direct circuit – Design and installation. Associação Brasileira de Normas Técnicas: Rio de Janeiro, Brasil, 2008.